

Monitoring Thermally-Induced Lesions with Supersonic Shear Imaging

J. BERCOFF, M. PERNOT, M. TANTER AND M. FINK

*Laboratoire Ondes et Acoustique (LOA)
ESPCI, C.N.R.S
UMR 7587, France*

*University Paris VII
Paris75005, France
jeremy.bercoff@loa.espci.fr*

Thermally-induced lesions are generally stiffer than surrounding tissues. We propose here to use the supersonic shear imaging technique (SSI) for monitoring high-intensity focused ultrasound (HIFU) therapy. This new elasticity imaging technique is based on remotely creating shear sources using an acoustic radiation force at different locations in the medium. In these experiments, an HIFU probe is used to generate lesions in fresh tissue samples. A diagnostic transducer, controlled by our ultrafast scanner, is located in the therapeutic probe focal plane. It is used for both generating the shear waves and imaging the resulting propagation at frame rates reaching 5,000 images/s. Movies of the shear wave propagation can be computed off-line. The therapeutic and imaging sequences are interleaved and a set of wave propagation movies is performed during the heating process. From each movie, elasticity estimations have been performed using an inversion algorithm. It demonstrates the feasibility of detecting and quantifying the hardness of HIFU-induced lesions using SSI.

KEY WORDS: Acoustic radiation force; elastography; HIFU; shear waves; supersonic regime.

INTRODUCTION

Real-time monitoring of HIFU treatments is a research field of major interest. In order to make HIFU clinically applicable, the use of monitoring methods of the treatment is crucial. Detecting a lesion as soon as it appears and monitoring its size are important requirements to avoid damage to surrounding healthy tissue .

Ultrasound imaging has been studied as a monitoring method¹ but has not been proven to provide robust lesion detection and characterization as it is mainly sensitive to the presence of bubbles in the lesion region generated by cavitation during the HIFU treatment.

A number of thermal imaging techniques have also been suggested and investigated. Magnetic resonance imaging (MRI) was the first imaging technique able to monitor HIFU ablation by providing temperature estimations during the treatment.^{2,3} However this technique is limited by its cost and lack of portability and may be not suitable for some patient populations. In order to overcome these limitations, ultrasound-based temperature imaging has been investigated. This last technique links a temperature elevation to ultrasound speckle changes in order to quantify the temperature in the medium.^{4,6} Compared to the MR temperature-imaging technique, it has low cost, high portability and can be easily integrated into an HIFU system. To date, this technique has not been proven to be reliable for the characterization of the induced lesion.

Another approach consists in characterizing the stiffness of the lesion, which is generally harder than the surrounding tissues.⁷ Several techniques based on this observation have been proposed. Among them, static elastography⁸ has been extensively investigated by several

groups and appear as an interesting solution for HIFU ablation monitoring of easy-access organ like prostate. In 1998, the use of static elastography for the visualization of HIFU induced thermal lesions was first investigated *in vitro* by Stafford et al,⁹ then by Kallel et al¹⁰ in the rabbit paraspinal skeletal muscle and by Righetti et al¹¹ in canine liver. *In vivo* tests were also reported by Varghese et al¹² on pig liver. Recently, the visualisation of HIFU-induced lesions in the human prostate was investigated *in vivo* by Souchon et al.¹³ For deep human organs like liver or brain, static elastography techniques cannot be used to date as monitoring technique for HIFU. In these cases, dynamic elastography techniques can be envisioned. Magnetic resonance elastography (MRE)¹⁴ and dynamic elastometry¹⁵ rely on monochromatic excitations. The first technique has been proven to be robust but has the limitations and inconveniences of MRI. Acoustic-radiation-force-based approaches are also currently under investigation. Lizzi et al¹⁶ and Fahey et al¹⁷ demonstrate promising preliminary *in vitro* and *ex vivo* results for HIFU monitoring after ablation. Konogafou et al¹⁸ have studied elasticity changes with temperature elevation in *ex vivo* samples. However, these techniques have a high exposure time to the radiation force pushing sequence and are intrinsically not quantitative.

We propose here to use the supersonic shear imaging technique^{19,20} to monitor elasticity during HIFU treatment before and after the necrosis threshold. Combining the advantages of transient elastography²¹ and the use of an acoustic radiation force, this technique is able to remotely generate and image shear waves in organs and then assess their elasticity in a few milliseconds. It has the advantage of being insensitive to motion artifacts and being able to reach, via the use of the radiation force, deep sited regions of interest.²⁰ In this work, an HIFU system has been coupled with an ultrasound-based imaging system. This imaging system is able to provide classical ultrasound images, temperature images and elasticity maps using SSI. Compared to other imaging systems (X ray CT, MR), it is a full ultrasound-based device, and therefore easily integrable into an HIFU system, with relatively low cost, high portability and real-time imaging capabilities. The imaging system allows us to control and compare SSI with the other monitoring techniques: ultrasound imaging and ultrasound temperature imaging. The latter technique has been validated to monitor heating processes below the necrosis threshold.⁶ This paper studies the feasibility of SSI for monitoring of temperature changes during an HIFU treatment as well as for the detection of tissue structural changes due to the appearance of a necrosis. The first section of the paper introduces and describes the supersonic shear imaging technique. In the second section, the experimental protocol coupling HIFU and the imaging system is presented. Finally the third section presents *in vitro* results of monitoring HIFU-induced lesions in a chicken breast sample. The shear modulus is found to be insensitive to temperatures changes before attaining the necrosis threshold. On the contrary, necrosed tissues are clearly detected by SSI revealing a strong increase of their shear modulus. The present study demonstrates the feasibility of using a fully ultrasound-based system combining two complementary imaging techniques, SSI and temperature imaging, to monitor, in real time, HIFU treatment before and after the necrosis threshold.

SUPERSONIC SHEAR IMAGING TECHNIQUE

SSI is a new ultrasound-based technique able to provide quantitative shear modulus mapping of an organ in less than 30 ms. SSI relies on the acoustic radiation force induced by an ultrasonic focused beam to remotely generate low frequency shear waves in tissues. It can be achieved using the same piezoelectric arrays such as the ones used in conventional ultrasonic

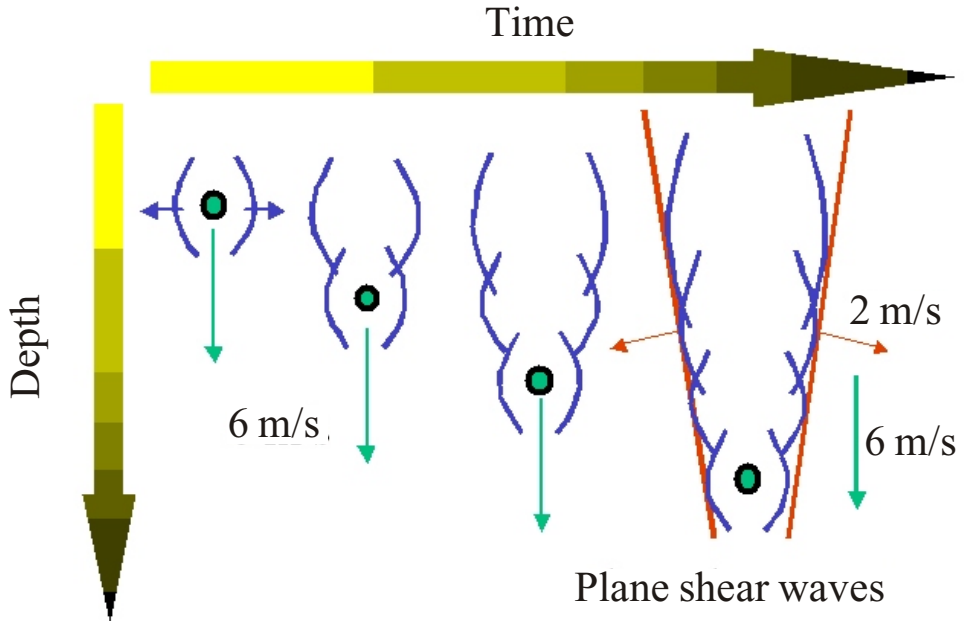


FIG. 1 Generation of the supersonic moving shear source. It results in the propagation of two plane shear waves propagating into a Mach cone.

scanners. Such a radiation force acts as a dipolar source of shear waves and mainly radiates in transverse directions. We propose, with SSI, to create quasi-plane shear waves of strong amplitude (40 to 100 μm displacement amplitude) by moving the shear source at a supersonic speed. Such a shear source, which moves faster than the shear waves, can be created by successively focusing the ultrasonic ‘pushing’ beam at different depths (Fig. 1). All resulting shear waves interfere constructively along a Mach cone creating two quasi-plane shear wavefronts propagating in opposite directions. The angle between both plane waves is proportional to the ratio between the speeds of the shear wave and moving source, i.e., to the Mach number. The ultrafast ultrasonic scanner developed for the technique is able to generate this supersonic shear source and image the propagation of the resulting transient plane shear waves. As those waves propagate through the medium in a few tens of milliseconds, frame rates of a few kHz are needed to capture their propagation. Such frame rates, not reachable with standard echographic devices, are possible with our ultrafast scanner as it reduces the emitting mode to a single plane wave insonification and realizes a parallel processing of all the lines (128) of the image. Establishing such a supersonic regime brings several essential innovations. First, constructive interferences between shear waves create a cumulative effect that induces high mechanical displacements in the medium (up to 100 μm in phantoms and 40 μm *in vivo*). This is an indispensable condition for the *in vitro* and *in vivo* feasibility of the technique, particularly in strongly viscous media (breast, liver). Secondly, the supersonic regime generates two spatially-extended plane shear waves, thus increasing the area where mechanical shear information is available. Finally, changing the speed of the moving ‘pushing’ beam allows us to change the Mach cone angle and then insonify the same medium with different steered plane waves. With this method, called shear compound, it is possible to gather the same mechanical information from different ‘points of view’ and therefore improve the robustness of the technique.

After the acquisition of echographic signals at an ultrafast frame rate (3 kHz), the data are transferred to a computer and the image sequence is formed. The displacements induced in

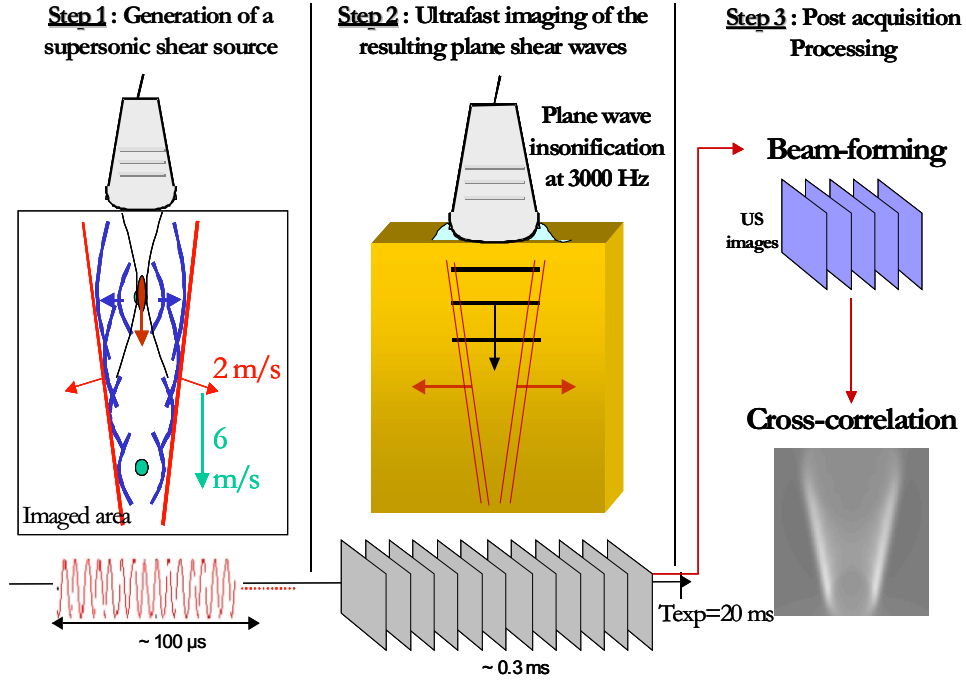


FIG. 2 Basic principles of supersonic shear imaging.

soft tissues by the shear waves propagation are estimated along the beam axis using a 1D cross-correlation algorithm between successive echographic images. The resulting movie shows the axial displacement induced by the shear wave during its propagation. The whole acquisition process and the signal processing is described in figure 2. The great versatility of our prototype allows the interleaving of ‘pushing sequences’ and ‘imaging sequences’ as desired. Images can then be acquired during the shear source movement to follow the generation of the Mach plane wave.

An experiment conducted in homogeneous Agar-Gelatin phantoms shows the ability of the system to generate and image the shear waves. The axial displacements are induced and measured using a 1D linear probe (128 elements, 4.3 MHz) located on the upper border of the images in figure 3. A Mach 3 supersonic regime was achieved as the shear wave speed is around $2 \text{ m}\cdot\text{s}^{-1}$ while the shear source is moved electronically by the array at $6 \text{ m}\cdot\text{s}^{-1}$. In order to generate the radiation force, the ultrafast scanner emits an ultrasonic focused beam in the phantom at five chosen locations (Fig. 2). The typical ultrasound pulse is made of 400 oscillations at 4.3 MHz. This corresponds to a ‘pushing time’ of $100 \mu\text{s}$. The shear waves propagates clearly in a Mach cone.

From the movie of these axial displacements, the elasticity map of the medium can be recovered by solving a local inverse problem. Assuming a medium that is purely elastic, infinite, isotropic and locally homogeneous, and that compressional waves are much faster than shear waves, we have shown that the spatio-temporal axial displacements at any location are linked in our transient experiments to the local shear modulus:

$$\frac{\partial^2}{\partial t^2} u(\vec{r}, t) = (\vec{r}) u(\vec{r}, t) \quad (1)$$

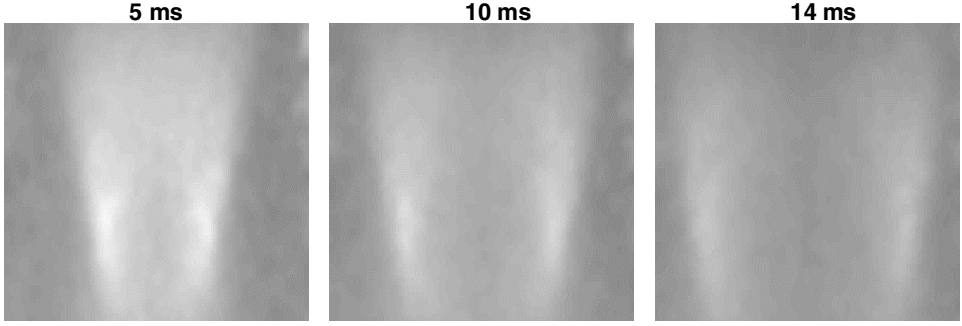


FIG. 3 Six images of the axial displacements induced in an agar-gelatin phantom. The acoustic radiation force source is moved electronically at 6 m.s⁻¹ by a 1D linear array located at the upper border of each image. The generated shear waves propagate at 2 m.s⁻¹ in the phantom, resulting in a Mach 3 experiment. The imaged represents a 40 * 40 mm² area.

where ρ is the density of the medium and can be considered as uniform in tissues. ∇^2 corresponds to the Laplacian operator. The inversion algorithm consists in locally estimating the shear modulus by inverting Eq. (1) in the Fourier domain:

$$G(x, z) = \frac{F \frac{\partial^2 u_z(x, z)}{\partial t^2}}{F \frac{\partial^2 u_z(x, z)}{\partial x^2} + \frac{\partial^2 u_z(x, z)}{\partial z^2}} \quad (2)$$

where F represents the Fourier transform in the time domain and ω the frequency window. The denominator represents the two-dimensional Laplacian operator. The third second-order spatial derivative along the array elevation axis is not measurable and is assumed to be zero. A complete study on the assumptions made and their implications are given in previous work.^{20, 21}

The inversion algorithm presented allows local and quantitative estimation of the shear modulus in the whole image region except in the source zone (where Eq. (1) is not true anymore). This has been demonstrated in calibrated tissue-mimicking phantoms^{20, 22} and is illustrated in figure 4 where the elasticity map of a 6 kPa phantom is shown. The sample was a homogeneous agar-gelatin phantom. Its 6 kPa elasticity was measured using a texture analyzer (Stable Micro Systems TA.XTplus) just before the SSI experiment. The resulting shear elasticity map shows a mean value of 6 kPa with a spatial standard deviation of 0.2 kPa.

MATERIALS AND METHODS

The experimental setup is presented in figure 5. A fresh sample of chicken breast was selected and placed in a water tank. The water and the chicken sample were degassed to avoid cavitation. A 60-element therapeutic probe controlled by our hyperthermia electronics is placed on one side of the tank. The supersonic shear imaging system is then placed to image the transverse focal plane of the HIFU transducer. Both sets of electronics were triggered to achieve the coupled experiments.

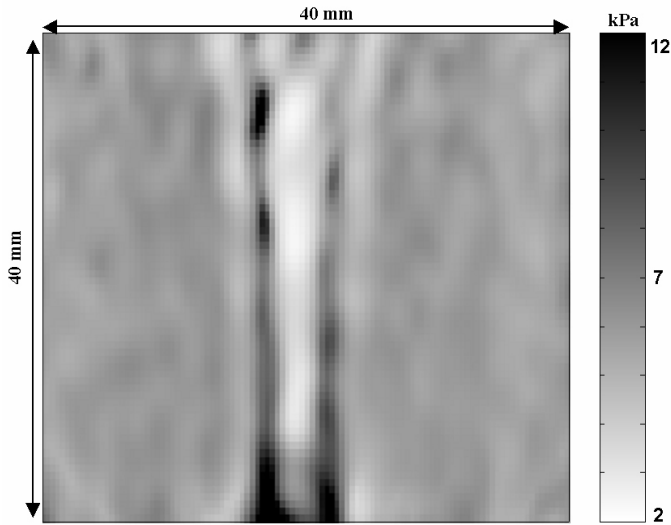


FIG. 4 Elasticity map of a 6kPa homogeneous tissue-mimicking phantom. The elasticity estimation is local and quantitative except in the source zone.

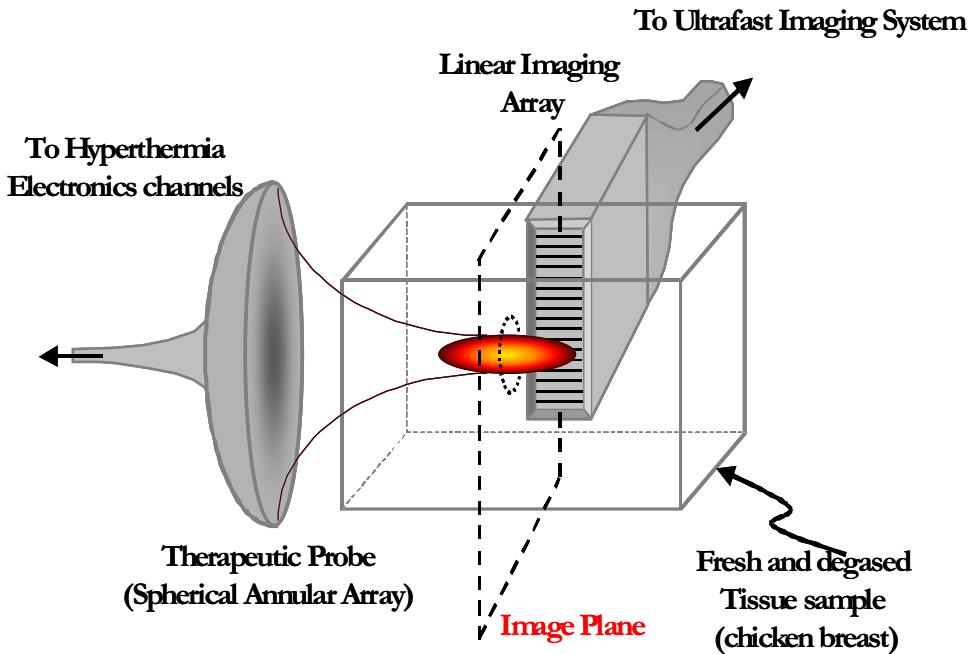


FIG. 5 Experimental setup. The supersonic shear imaging system is imaging the transverse focal plane of an HIFU system.

HIFU system

The therapeutic probe used for the experiment is a 1.5 MHz annular array with 60 elements and a maximum focal intensity of $1,000 \text{ W/cm}^2$. The HIFU spot is 1.7 mm diameter in the focal plane and has a 7.5 mm length in the axial plane. The electronics controlling the

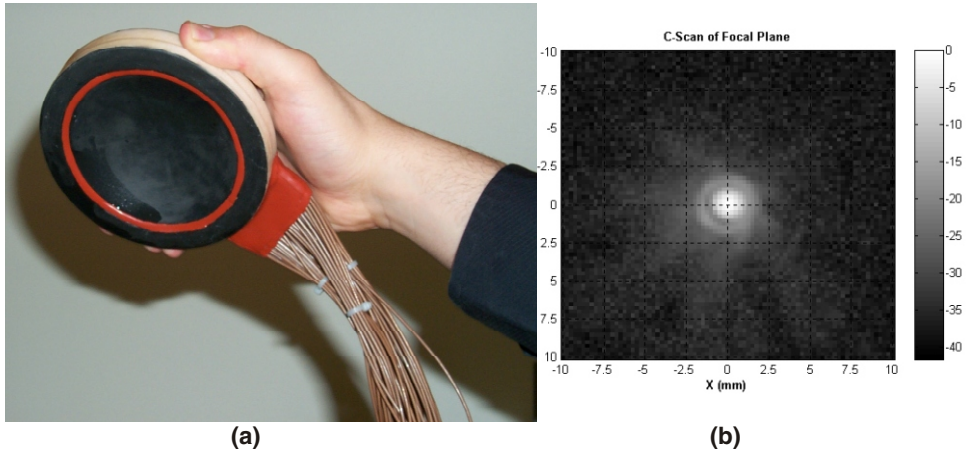


FIG. 6 (a) Therapeutic probe. (b) Geometry of its focal spot (in dB).

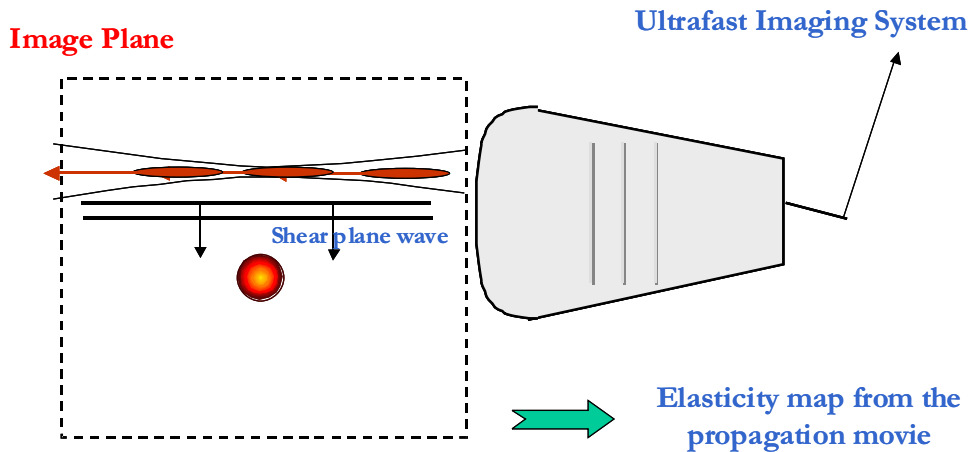


FIG. 7 Experimental setup. The supersonic shear imaging system is imaging the transverse focal plane of an HIFU system.

probe is made of 200 independent and programmable channels with an 80 V peak-to-peak voltage (only 60 were used for this experiment). Figure 6 shows a picture of the probe and the geometrical characteristics of the pressure field pattern that it induces in water.

Imaging system

The imaging system consists of a classical ultrasonic array (1D linear array with a center frequency of 4.3 MHz) linked to the ultrafast ultrasonic scanner. This system is able to compute classical ultrasound images, temperature images using an ultrasound-based compound technique developed in our lab and elasticity maps using SSI. A complete technical description of this fully programmable multichannel system is provided in reference [?](#). This system will be used to monitor HIFU treatment during the heating process and after lesion generation. A view of the experiment in the image plane is shown in figure 7.

To compute an elasticity map, the ultrafast scanner induces a supersonic moving source on one side of the thermal focal spot and images the propagation of the resulting shear wave

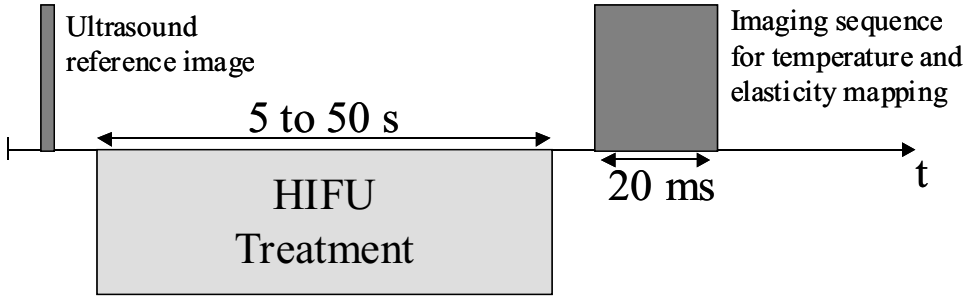


FIG. 8 Acquisition sequence of the coupled and triggered system.

while it passes through the thermal spot. Then, by processing the data as described in the previous section, an elasticity map of the heated zone can be computed.

Experimental protocol

Two experiments were performed. The first experiment was designed to study the evolution of elasticity in the heated region with temperature. The HIFU probe induces a set of heating sequences with different insonification times. The insonification time was varied from 5 to 50 s with a 5 s step. For all sequences, the maximum focal intensity was fixed at 250 W/cm^2 . After each heating sequence, ultrasound images were acquired by the ultrafast ultrasonic scanner and temperature and elasticity images of the heated zone were computed. Temperature images were calculated using an ultrasound-based technique that estimates the speckle motion due to thermal expansion and local changes in the speed of sound during a heating process. Such a technique is quantitative in the temperature window considered. Figure 8 shows a typical acquisition sequence for this first experiment.

The second experiment was designed to study the ability of SSI to detect HIFU-induced lesions. The heating sequence was increased to deposit $1,000 \text{ W.cm}^{-2}$ at the focus and the insonification time was increased to 10 successive bursts of 5 s each in order to reach the necrosis threshold. An elasticity map of the region of interest was realized using SSI just after the heating sequence.

Signal processing

For both sets of experiments, the elasticity maps were computed using the inversion algorithm presented in section I. However, the acquired data have to be filtered to make the inversion relevant. First, the calculated spatio-temporal displacements are spatially filtered using a 2D spatial Gaussian low pass filter. These smoothed displacements are used to calculate the second spatial and temporal derivatives. Finally, Eq. (2) is applied using a frequency window around the shear wave center frequency in which the Laplacian spectrum has values beyond a chosen threshold. This regularization step eliminates values in areas where the Laplacian term is too weak and is equivalent to a temporal filter.

RESULTS

For the first experiment where the heating process was conducted without reaching the necrosis threshold, temperature and elasticity images were computed after each heating sequence. A typical temperature image (resulting from a 30 s heating process) is shown in figure 9(a) and shows clearly a cross-section of the HIFU beam. It has been superimposed

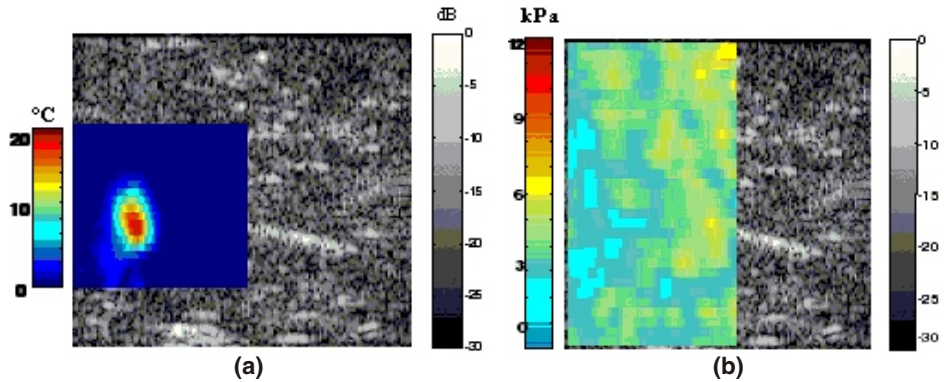


FIG. 9 (a) Map of the temperature increase superimposed on the echographic image of the breast chicken tissue sample. In this first set of experiments, the necrosis threshold was not reached. The image size is 40 x 40 mm². (b) Elasticity map superimposed on the echographic image calculated after a 20°C heating.

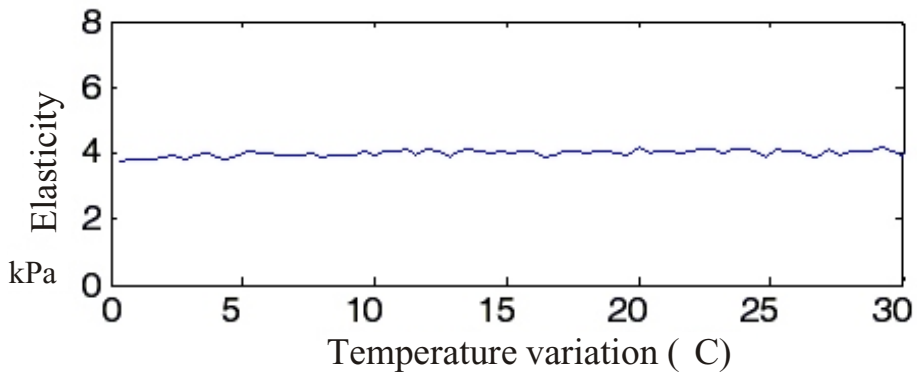


FIG. 10 Mean elasticity variations with temperature.

on an echographic image of the tissues sample achieved with the 1D linear imaging array. The set of temperature images allows the calculation of the temperature reached at focus as a function of the insonification time. The insonification times used corresponds to a temperature variation of 30° C (from 20 to 50°C) with a 5°C step. During these first sets of experiments, we did not notice a significant change in the shear modulus of the heated region. A typical shear modulus map of the heated region is given figure 9(b). The map is relatively homogeneous with 4 kPa mean value and a 4% spatial variance. No shear elasticity changes are noticeable in the zone presenting a temperature increase on the temperature image.

The mean elasticity has been calculated for each heating process and plotted as a function of the measured temperature (at focus). The plot is shown figure 10 and does not reveal any noticeable variation. Those results, in the temperature window considered are in pretty good agreement with results obtained by Konofagou et al using MR temperature imaging.¹⁸

This small dependence of the shear modulus versus temperature before necrosis can be intuitively explained by the fact that null divergence motion induces less temperature changes than null rotational motion. In other words, the temperature dependence of compressional wave speed seems to be more important than the one of shear wave speed. This point will be developed in further work.

In the second experiment, the necrosis threshold has been reached. Figure 11(a) presents a picture of the tissue sample cut in slices in order to highlight the necrosis region. The size of the imaging area of the 1D linear array is described by the black rectangle. The necrosis is

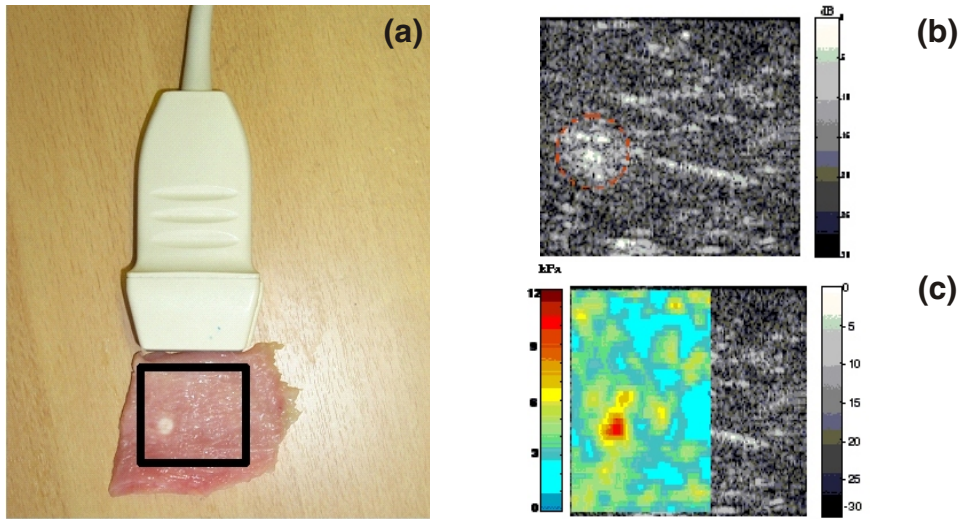


FIG. 11 (a) Picture of the lesion induced in a tissue sample and corresponding imaged area. (b) Echographic image just after HIFU treatment. The imaged area size is $40 \times 40 \text{ mm}^2$. (c) Map of the shear modulus achieved using the supersonic imaging technique superimposed on the echographic image after necrosis.

clearly visible on the left side of the rectangle and has a 5 mm diameter. Figure 11(b) shows the ultrasound image of the sample acquired just after the HIFU sequence. The necrosis region present high reflectivity due to the presence of bubbles induced by the HIFU treatment. This brighter zone, which is wider than the necrosis itself, tends to disappear after a few seconds, making the necrosis undetectable in ultrasound images. Ultrasound-based temperature images are not accurate anymore due to the fact that the lesion induces speckle decorrelation, making the measurement irrelevant. For this reason, they have not been computed. Figure 11(c) represents the shear modulus map obtained using SSI, which has been scaled and superimposed on the ultrasound image.

The elasticity map, which has been scaled between 0 and 12 kPa, clearly shows two distinct zones. The necrosed area appears harder than the surrounding tissues. The shear modulus in the untreated zone has mean value of 4.1 kPa with spatial standard deviation of 0.3 kPa. Those value are similar to the ones found in the previous experiment before having induced the necrosis.

In order to study the geometry and elasticity of the necrosed area, the mean value of the untreated zone (4.1 kPa) has been subtracted from the absolute elasticity map (Fig. 11). Then, this rescaled elasticity map has been normalized. The size of the necrosis has been defined as the width at half amplitude level (-6 dB). The mean elasticity of the necrosis has been defined as the mean value of the elasticity map in the zone inside the defined boundaries. Plots of the normalized elasticity as a function of the lateral and axial positions are shown respectively in figures 12(b) and (c). Figure 12(a) represents a zoom in the picture of the necrosed chicken sample. It indicates the axes (x and z) on which the elasticity has been studied. A reference estimation of the geometry of the necrosed area can be performed by simply studying the optical properties of the sliced *ex vivo* sample. The *ex vivo* picture of the necrosed sample has been converted into gray scale levels. Plots of the normalized gray scale levels of the picture as a function of the lateral and axial positions are also showed in figures 12(b) and (c) and superimposed to the normalized elasticity plots. Both set of curves exhibit a good correlation. Estimated on the elasticity curves picture, the necrosis has respectively $4.1 \pm 0.1 \text{ mm}$ length along the lateral position and a $4.3 \pm 0.2 \text{ mm}$ length along the axial one. Those values are in good agreement with the lesion size measured on the grayscale plots – 4.7 mm (lateral)

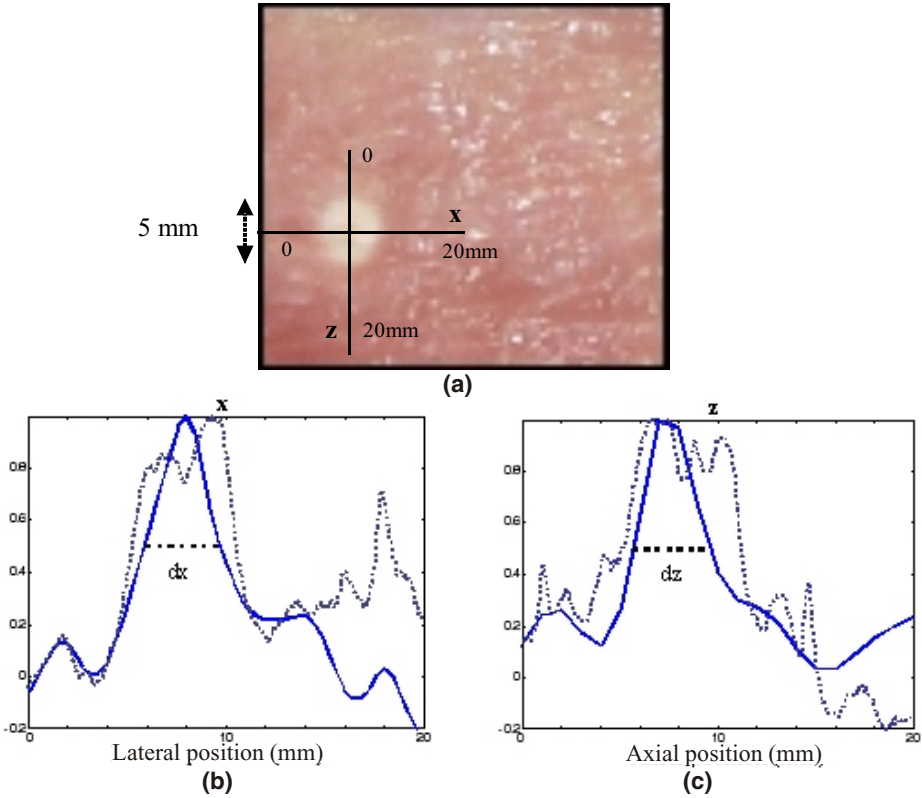


FIG. 12 (a) Zoom on the lesion induced in the chicken sample showing the axis where the elasticity has been studied. (b) Elasticity and optical properties as a function of the lateral position. (c) Elasticity and optical properties as a function of the axial position.

and 5.8 mm (axial). This demonstrates that there is a strong correlation between the elasticity map provided by SSI and the optical properties map in the necrosed area. Note that the elasticity map gives a lesion slightly smaller (with the size definition chosen) than the optical one due to the fact that the edges of the lesion are not as sharp as in the optical picture; a gradient of elasticity is clearly visible. It is not possible to certify the validity of this gradient because of two approximations made in the elasticity computation. First, the inversion algorithm is not true at the edges of the necrosis, leading to a local wrong elasticity estimation (the medium has been assumed locally homogeneous). Secondly, this error is slightly blurred on a few pixels (i.e., about 1 mm) due to the spatial filter applied to the data before inversion. This explains why the lesion size, if defined at -12 dB, fits perfectly the optical estimation while if defined at -6 dB (as chosen here for better coherence) is slightly underestimated. However these differences become negligible as the lesion size increases. By the way, these approximations do not significantly affect the quality of the reconstruction; the necrosis is clearly detected and its elastic geometry is pretty well correlated to the optical one. Finally, the mean elasticity in the necrosis is 10.5 ± 0.2 kPa. The shear modulus ratio between the necrosis and untreated area is 2.6. The characteristics of the lesions (size and elasticity) and its corresponding variance has been calculated with a set of four slices of the same chicken breast in which the same HIFU treatment has been performed. In this experiment no other calibrated technique has been applied to confirm those shear modulus values. However, SSI has been proven to be quantitative in calibrated elastic phantoms¹³ and the contrast ratio between the lesion and surrounding tissues is in good agreement with the first *in vivo* results

obtained on prostate by Souchon et al¹³ using static elastography. The strain contrast ratio between necrosed and healthy tissues was found to be between 0.32 and 0.56 and can be considered as equivalent to the inverse of the shear modulus ratio if the stress applied is assumed locally homogeneous in the area of interest. One should note that SSI is capable here of detecting and mapping a 5 mm necrosis, i.e., as large as a quarter of the shear wavelength. Such results emphasize the fact that the inversion algorithm is not limited by the shear wavelength as it is usually the case for the inverse problem in seismology, for example. The shear wave propagation is measured in the bulk and not only on a surface surrounding the medium. Consequently, at each location inside the medium, the complete displacement field is measured, including evanescent waves, which contain details of the medium much smaller than the wavelength. This is a hyperresolution property of our inversion process. However, if theoretically the ultimate resolution of the technique is given by the echographic image resolution, this is not perfectly true for *in vitro* conditions where the applied spatial filtering mentioned in the previous section degrades the spatial resolution. The technique can here rely here on a spatial resolution of 1 to 2 mm² which is enough to detect the 5 mm inclusion.

The feasibility of using supersonic shear imaging to detect a necrosis and estimate its hardness was demonstrated *in vitro*. However a more precise study on the variation of shear elasticity with temperature needs to be done for higher temperature (from 50°C to the complete formation of the necrosis). Such a study, which represents the link between both experiments that were presented, was not possible using the techniques reported here. For temperatures higher than 50 °C, the necrosis starts to appear at focus of the HIFU probe in chicken breasts, inducing a high level of speckle decorrelation. The ultrasound-based temperature estimation is not reliable anymore. This study will be presented in future work.

The next step will consist in embedding a 1D linear array inside a new HIFU spherical multichannel probe, thus providing a more flexible and compact probe, mixing both therapy and monitoring of thermal and elasticity changes during the HIFU treatment. The mixed system is currently being designed at the laboratory and will be used in the next months to induce and detect lesions *in vivo* in the brain of a set of 20 sheep.

SUMMARY AND CONCLUSIONS

The combination of the acoustic radiation force and ultrafast imaging mode in order to respectively remotely generate shear waves in the organs and image their propagation allows the recovery of the shear modulus image of soft tissues. This technique, called supersonic shear imaging, was applied *in vitro* on chicken breast tissue samples in order to monitor the elasticity change during an HIFU insonication. Before attaining the necrosis threshold, no significant change in the shear elasticity estimates was noticed. After attaining necrosis, the shear modulus was three times higher in the necrosed area and the necrosed area was clearly highlighted. Ultrasound temperature imaging has been shown to be an interesting method to follow the treatment before the necrosis threshold. Supersonic shear imaging appears to be a promising ultrasound-based technique for the monitoring of HIFU-induced lesions. Future work will consist in validating *in vivo* the use of the technique for detecting lesions on sheep brains. The goal will be to demonstrate the feasibility of building a fully ultrasound-based system mixing therapy (with HIFU) and diagnostic capabilities (with ultrasound imaging, temperature imaging and viscoelasticity imaging).

REFERENCES

1. Gertner MR, Worthington AE, Wilson BC, Sherar MD. Ultrasound imaging of thermal therapy in *in vitro* liver, *Ultrasound Med Biol* 24,1023-1032 (1998).

2. Cline H, Hynynen K, Hardy C, et al. MR temperature mapping of focused ultrasound surgery, *Magn Reson Med* 31, 628-636 (1994).
3. McDannold, King, NL., Jolesz F, Hynynen K. Usefulness of MR imaging-derived thermometry and dosimetry in determining the threshold for tissue damage induced by thermal surgery in rabbits, *Radiology* 216, 517-523 (2000).
4. Seip R, Ebbini E. Noninvasive estimation of tissue temperature response to heating fields using diagnostic ultrasound, *IEEE Trans Biomed Eng* 42, 828-839, (1995).
5. Simon C, VanBaren P, Ebbini E. Two-dimensional temperature estimation using diagnostic ultrasound, *IEEE Trans Ultrason Ferroelec Freq Contr* 45, 1088-1099 (1998).
6. Pernot M, Tanter M, Bercoff J, Waters K, Fink M. Temperature estimation using ultrasonic spatial compound imaging, *IEEE Trans Ultrason Ferroelec Freq Contr* (in press).
7. Krouskop E, Wheeler T, Kallel F, Garra B, Hall T. Elastic moduli of breast and prostate tissues under compression, *Ultrasonic Imaging* 20, 260-274 (1998).
8. Ophir J, Cespedes EI, Ponnekanti H, Yazdi Y, Li X. Elastography: a quantitative method for imaging the elasticity of biological tissues. *Ultrasonic Imaging* 13, 111-134 (1991).
9. Stafford RJ, Kallel F, Price RE, et al. Elastographic imaging of thermal lesions in soft tissue: a preliminary study *in vitro*, *Ultrasound Med Biol* 24, 1449-1458 (1998).
10. Kallel F, Stafford RJ, Price, RE, et al. The feasibility of elastographic visualization of HIFU-induced thermal lesions in soft tissues. Image-guided high-intensity focused ultrasound, *Ultrasound Med Biol* 25, 641-647 (1999).
11. Righetti R, Kallel F, Stafford RJ, et al. Elastographic characterization of HIFU-induced lesions in canine livers, *Ultrasound Med Biol* 25, 1099-1113 (1999).
12. Varghese T, Zagzebski JA, Lee FT. Elastographic imaging of thermal lesions in the liver *in vivo* following radiofrequency ablation: preliminary results, *Ultrasound Med Biol* 28, 1467-1473 (2002).
13. Souchon R, Rouviere O, Gelet, A, et al. Visualisation of HIFU lesions using elastography of the human prostate *in vivo*: preliminary results, *Ultrasound Med Biol* 29, 1007-15 (2003).
14. Wu, T, Felmlee JP, Greenleaf JF, Riederer SJ, Ehman RL. Assessment of thermal tissue ablation with MR elastography, *Magnetic Reson Med* 45, 80-87 (2001).
15. Shi X, Martin RW, Rouseff D, Vaezy S, Crum LA, Detection of high-intensity focused ultrasound liver lesions using dynamic elastometry, *Ultrasonic Imaging* 21, 107-26 (1999).
16. Lizzi FL, et al. Radiation-force technique to monitor lesions during ultrasonic therapy, *Ultrasound Med Biol* 29, 1593-1605 (2003).
17. Fahey, BJ, Nightingale KR, Stutz DL, Trahey GE. Acoustic radiation force impulse imaging of thermally- and chemically-induced lesions in soft tissues: preliminary *ex vivo* results, *Ultrasound Med Biol* 30, 321-328 ().
18. Konofagou E, Thierman J, Hynynen K. The use of ultrasound-stimulated acoustic emission in the monitoring of modulus changes with temperature, *Ultrasonics* 41, 337-345 (2003).
19. Bercoff J, Tanter M, Fink M, Sonic boom in soft materials: the elastic cerenkov effect, *Applied Phys Lett* 84, 2202-2204 (2004)
20. Bercoff J, Tanter M, Fink M, Supersonic Shear Imaging: a new technique for soft tissue elasticity mapping, *IEEE Trans Ultrason Ferroelec Freq Contr* 51, 374-409 (2004).
21. Bercoff J, Chaffai S, Tanter M, et al. *In Vivo* breast tumor detection using Transient Elastography, *Ultrasound Med Biol* 29, 1387-1396 (2003).
22. Sandrin, L., Tanter, M., Catheline, S., Fink, M., Shear modulus imaging with time resolved 2D pulsed Elastography, *IEEE Trans Ultrason Ferroelec Freq Contr* 49, 426-435 (2002).
23. Shattuck D. ExplosoScan: a parallel processing technique for high speed ultrasound imaging with linear phased arrays, *J Acoust Soc Am* 75, 1273-1282 (1984).
24. Bishop J, Poole G, Leitch M, Plewes DB, Magnetic resonance imaging of shear wave propagation in excised tissue, *J Mag Reson Imag* 8, 1257-1265 (1998).

two more
authors
needed

year?